Fatigue & Fracture of
Engineering Materials & Structures

doi: 10.1111/j.1460-2695.2011.01628.x

Fracture toughness and growth of short and long fatigue cracks in ductile cast iron EN-GJS-400-18-LT

H. R. ZAMBRANO[1], G. HÄRKEGÅRD[1] and K. F. STÄRK[2]

[1]*Department of Engineering Design and Materials, Norwegian University of Science and Technology, NO-7491 Trondheim, Norway,*
[2]*ALSTOM (Switzerland) Ltd., Switzerland*

Received in final form 9 August 2011

ABSTRACT Heavy components of ductile cast iron frequently exhibit metallurgical defects that behave like cracks under cyclic loading. Thus, in order to decide whether a given defect is permissible, it is important to establish the fatigue crack growth properties of the material. In this paper, results from a comprehensive study of ductile cast iron EN-GJS-400-18-LT have been reported. Growth rates of fatigue cracks ranging from a few tenths of a millimetre ('short' cracks) to several millimetres ('long' cracks) have been measured for load ratios $R = -1$, $R = 0$ and $R = 0.5$ using a highly sensitive potential-drop technique. Short cracks were observed to grow faster than long cracks. The threshold stress intensity range, ΔK_{th}, as a function of the load ratio was fitted to a simple crack closure model. Fatigue crack growth data were compared with data from other laboratories. Single plain fatigue tests at $R = -1$ and $R = 0$ were also carried out. Fracture toughness was measured at temperatures ranging from $-40\ ^{\circ}$C to room temperature.

Keywords ductile cast iron; fatigue crack growth; fatigue limit; fracture toughness; threshold stress intensity range.

NOMENCLATURE

A = elongation
a = crack depth
a_i = initial crack depth
a_f = final crack depth
a_0 = intrinsic crack depth
C = coefficient in crack growth law
D = mean graphite nodule diameter
d = notch depth
da/dN = fatigue crack growth rate
E = modulus of elasticity
F = crack geometry factor
$\mathcal{J}_{Ic}$ = fracture toughness expressed in terms of the $\mathcal{J}$-integral
$K_{\mathcal{J}IC}$ = (fictitious) fracture toughness expressed in terms of the stress intensity factor obtained from $\mathcal{J}_{Ic}$ assuming linear elastic conditions
$K_{P_{max}}$ = stress intensity factor at the maximum force (final fracture)
K_Q = stress intensity factor determined at P_Q
M = mean stress sensitivity
m = exponent in crack growth law
N = number of cycles

Correspondence: H. R. Zambrano, E-mail: habib.zambrano@ntnu.no

P_Q = force at deviation from linearity in force versus displacement as defined by ASTM Standard E1820 for fracture toughness testing
ν = Poisson's ratio
R = load ratio
R_{op} = load ratio, above which the fatigue crack remains fully open
R_m = tensile strength
$R_{p0.2}$ = 0.2% proof strength
T = temperature
u = relative potential drop increase
V = potential drop over cracked specimen
V_0 = potential drop over notched (crack free) specimen
W = specimen width
y = distance between potential probe and crack plane
Z = reduction of area
Δa = crack increment
ΔK = stress intensity range
$\Delta K_{eff,th}$ = threshold stress intensity range of fully open crack
ΔK_{eq} = equivalent stress intensity range (short-crack corrected)
ΔK_{th} = threshold stress intensity range
ΔN = number of cycles to propagate a fatigue crack an increment Δa
ΔS = gross nominal stress range
$\Delta \sigma$ = stress range
$\Delta \sigma_A$ = median plain fatigue limit (stress range)
$\Delta \sigma_W$ = median plain fatigue limit under alternating stress, $R = -1$
ρ = notch root radius
σ_m = mean stress

INTRODUCTION

The steady increase in the number and size of wind turbines for the generation of electric power requires improved knowledge of materials data for highly loaded components. Ductile cast iron EN-GJS-400-18-LT[1] is widely used for wind-turbine hub, bearing housing and base plate. Even in components cast under optimized conditions, the designer must allow for the presence metallurgical defects, e.g. shrinkage cavities, porosity, slag inclusions and degenerate graphite. Under cyclic loading conditions, such defects tend to behave as cracks. Hence, the endurance of cast components is mainly controlled by the growth of fatigue cracks from casting defects.[2–7] To be able to determine the size of permissible defects for a given endurance, the designer needs access to reliable fatigue crack growth (FCG) data. For ductile cast iron EN-GJS-400-18-LT, the availability in the open literature of such data is still very limited.[8–10] Besides, available data typically refer to tests on several-millimetre-long cracks. In many cases, however, fatigue life is dominated by the growth of sub-millimetre cracks.[2,7] Therefore, in the present investigation, FCG tests have been carried out on cracks ranging from a few tenths of a millimetre ('short' cracks) to several millimetres ('long' cracks). Previous FCG tests have been limited to positive load ratios, $R > 0$, whereas wind turbine load spectra contain a considerable fraction of load cycles with $R < 0$. Thus, this study includes tests at $R = -1$.

Although not of primary importance in fatigue life assessment, it was decided to supplement the FCG tests with fracture toughness measurements at a range of temperatures.

MICROSTRUCTURE AND TENSILE PROPERTIES

In this research, test specimens taken out of a 40 mm × 80 mm × 635 mm rectangular block of ductile cast iron EN-GJS-400-18-LT, with a chemical composition as given in Table 1, have been investigated. The microstructure of the material is characterized by spheroidal graphite nodules embedded in a ferritic matrix as shown in Fig. 1. The size distribution of the graphite nodules, determined by measuring 790 nodules with diameters ranging between 10 μm and 120 μm, is shown in Fig. 2. The

Table 1 Chemical composition (wt.%) of ductile cast iron EN-GJS-400-18-LT, balance Fe

C	Si	Mn	P	S	Ni	Mg
3.61	2.18	0.23	0.014	0.009	0.088	0.041

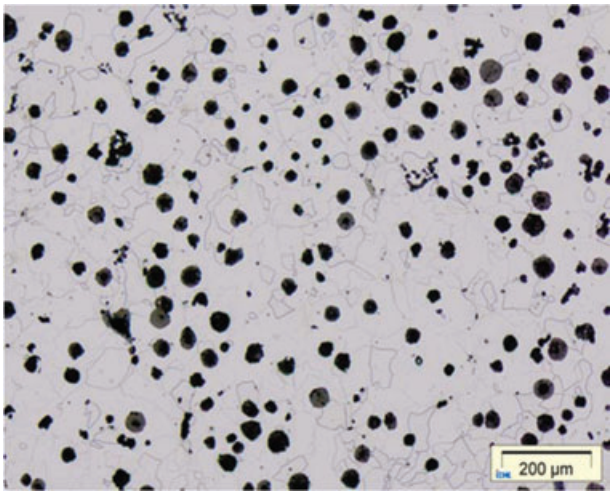

Fig. 1 Microstructure of ductile cast iron EN-GJS-400-18-LT.

arithmetic mean was found to be $D = 32$ μm, the standard deviation 16 μm.

A cylindrical sample of this material with diameter 21 mm and gage length 100 mm was examined for defects by means of X-ray computed tomography (XCT).[11] No defects were found above the XCT resolution limit of 0.2 mm.

Hardness and tensile properties of the cast block were measured at room temperature. In good agreement with Ref. [1], the hardness was found to be 150 HB 2.5/187.5.

Table 2 Mean graphite nodule diameter (D) and tensile properties of ductile cast irons similar to EN-GJS-400-18-LT

Material	D (μm)	R_m (MPa)	$R_{p0.2}$ (MPa)	Z (%)	A (%)	E (GPa)
WKN[8]	60	403	245	16	22	171
Tokaji[9]	54	400	274	10	7	142
WK2[8]	37	382	256	23	18	170
Present study	32	402	260	26	28	166
WK1[8]	23	396	265	21	23	173
Berdin[12]	20	390	260	23	19	187
Clement[13]	17	450	270	8	–	–

The tensile properties of the cast block, $R_m = 402$ (390) MPa, $R_{p0.2} = 260$ (230) MPa and $Z = 28$ (15)%, satisfy the standard requirements (in brackets).[1] Tensile properties and the mean graphite nodule diameter reported for ductile cast irons of the same type have been listed in Table 2. Figure 3 shows that R_m and $R_{p0.2}$ are virtually independent of the nodule size.

FRACTURE TOUGHNESS

The resistance of the ductile cast iron EN-GJS-400–18-LT to brittle fracture was determined by means of two different specimen geometries: single-edge bend SE(B) and compact C(T) specimens as depicted in Fig. 4a and b, both 10-mm thick. For these small specimens to yield consistent results, it was necessary to use side grooves. These constrain the deformation around the crack tip at the surface of the specimen, thus creating a more homogeneous stress state through the thickness.[14] Crack mouth opening displacement was measured by means of a clip gage across the notch as shown in Fig. 5a. This figure also shows the cooling equipment required to measure

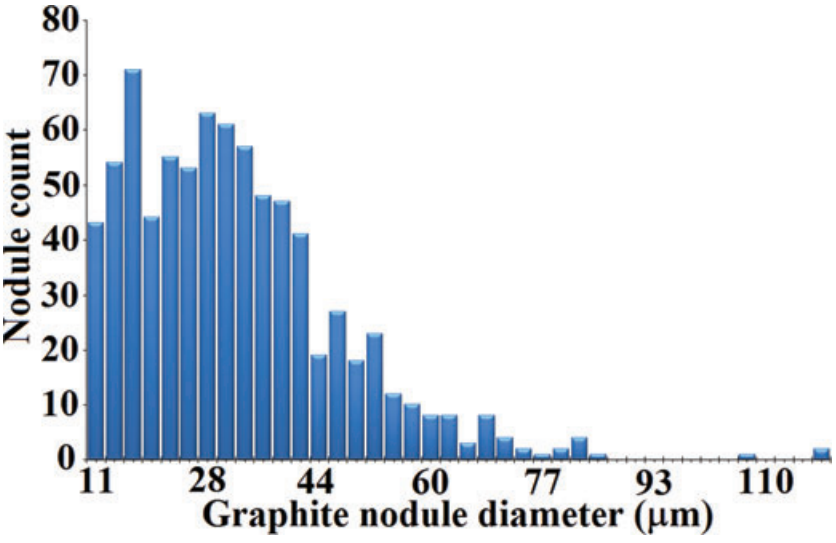

Fig. 2 Nodule size distribution for ductile cast iron EN-GJS-400-18-LT.

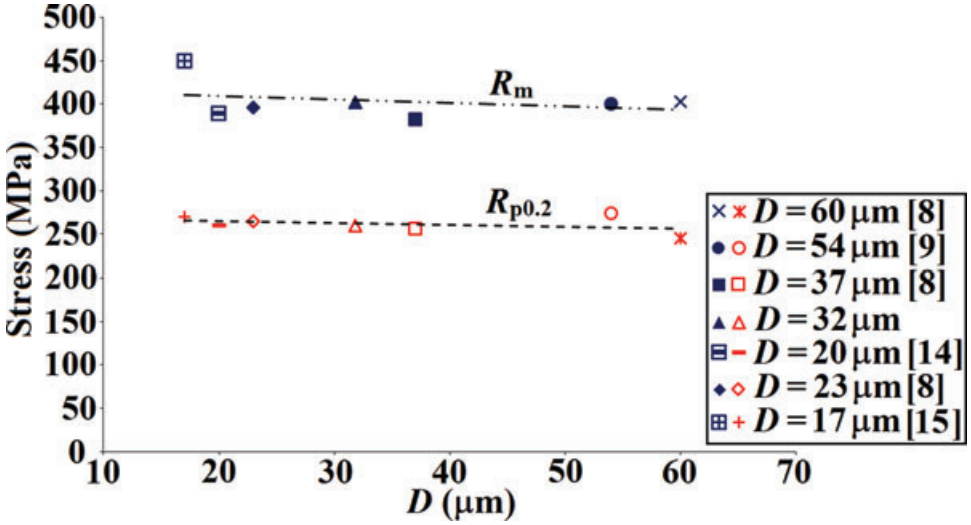

Fig. 3 Influence of the mean graphite nodule diameter on R_m and $R_{p0.2}$ for GJS-400-type ductile cast iron.

fracture toughness below room temperature. The crack extension was monitored by means of the potential drop method.

The fracture toughness expressed in terms of the $\mathcal{J}$-integral, $\mathcal{J}_{Ic}$, was determined in accordance with the ASTM Standard E1820.[15] A (fictitious) fracture toughness expressed in terms of the stress intensity factor obtained from $\mathcal{J}_{Ic}$ assuming linear elastic conditions was determined as $K_{\mathcal{J}_{Ic}} = \sqrt{\mathcal{J}_{Ic} E/(1-\nu^2)}$. By-products from the ASTM measurement procedure are the stress intensity factor at the maximum force (final fracture), $K_{P_{max}}$, and that at the force P_Q as defined in Fig. 5b, K_Q.

$K_{P_{max}}$, K_Q and $K_{\mathcal{J}_{Ic}}$ were determined for the material under investigation at temperatures between −38 °C and 22 °C. The experimental results have been summarized in Table 3 and Fig. 6. The room temperature values of $K_{\mathcal{J}_k}$ are in good agreement with $K_{\mathcal{J}_{Ic}} = 71\ \text{MPa}\sqrt{\text{m}}$ based on unpublished data due to Hübner et al., cf.[8]. It should be noted that fracture toughness remains nearly constant over the investigated range of temperatures.

THE PLAIN FATIGUE LIMIT AND ITS MEAN STRESS DEPENDENCE

In order to determine the fatigue limit of axially loaded plain specimens, a load-increasing procedure due to Denk and Amhof[16] was used. Plain specimens ($d = 0$) as shown in Fig. 7a were tested at $R = -1$ and $R = 0$ by means of a horizontal resonance testing machine with water-cooled grips and a capacity of 20 kN. Each specimen was tested at 110 Hz at a stress amplitude initially below the expected fatigue limit. As shown in Fig. 7b, the stress amplitude was increased by 2% every 200 000 cycles. When a crack had initiated and become sufficiently deep to markedly decrease the resonance frequency of the testing system, the test was terminated.

The plain fatigue limits obtained under axial loading are $\Delta\sigma_A(R=-1) = \Delta\sigma_W = 362$ MPa (push–pull) and $\Delta\sigma_A(R = 0) = 292$ MPa (zero-to-tension); see also Fig. 8 and Table 5. The push–pull fatigue limit is in fair agreement with the fatigue limit under rotating bending stated in [Ref. 1], $\Delta\sigma_W = 390$ MPa. The observed difference may be explained in terms of stress–gradient and weakest-link arguments[17,18].

Kaufmann and Wolters[19] used the parameter

$$M = \frac{\Delta\sigma_A(R=-1)}{\Delta\sigma_A(R=0)} - 1, \tag{1}$$

to quantify the mean stress sensitivity of GJS-400-type ductile cast iron. For fatigue test specimens with regular graphite nodules and (small) embedded shrinkage cavities, they found M to be in the range 0.23–0.29. The mean stress sensitivity of the present material, $M = 0.24$, is within this range, giving support to the tomographic observation that no defects > 0.2 mm could be found in a sample of the casting.

The effect of mean stress on the fatigue limit has traditionally been described by the (modified) Goodman equation

$$\frac{\Delta\sigma}{\Delta\sigma_W} + \frac{\sigma_m}{R_m} = 1. \tag{2}$$

This equation yields a conservative prediction of the fatigue limit at $R = 0$. A perfect fit to the experimental value is obtained by replacing the linear mean-stress term by a power term, i.e.

$$\frac{\Delta\sigma}{\Delta\sigma_W} + \left(\frac{\sigma_m}{R_m}\right)^{\delta} = 1, \tag{3}$$

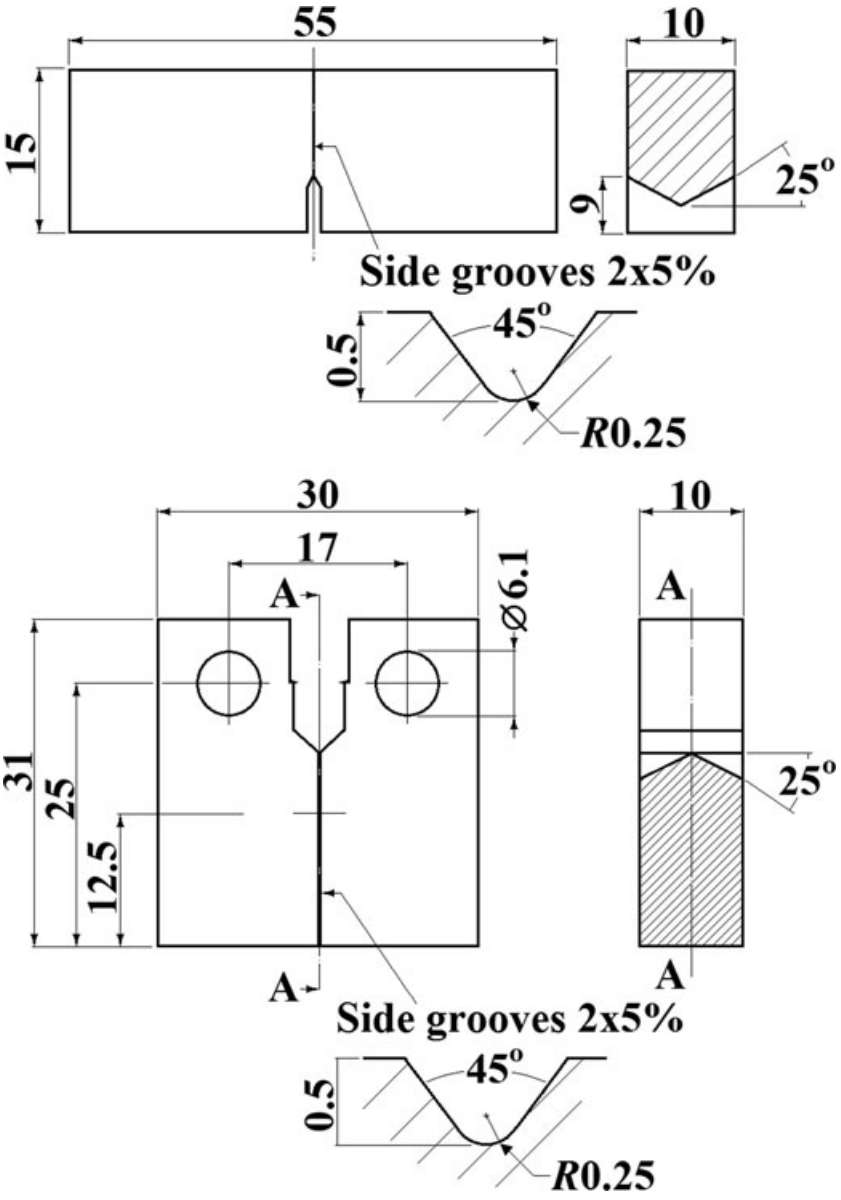

Fig. 4 (a) Single-edge bend SE(B) and (b) compact C(T) specimen.

where $\delta = 1.62$. It may be noted that Eq. (3) reproduces the well-known Gerber parabola,[18] when $\delta = 2$. Clearly, because data are only available for $R = -1$ and 0, Eq. (3) can only be expected to be accurate for $-1 \leq R \leq 0$, and extrapolation to $R > 0$ is fraught with uncertainty. However, as $\Delta\sigma_A$ for $R = -1$, 0 and 0.5 will be needed in an attempt to model the growth of short fatigue cracks, Eq. (3) has been used to estimate $\Delta\sigma_A(R = 0.5) = 177$ MPa.

FATIGUE CRACK GROWTH TESTING

FCG tests were carried out on specimens with a starter notch as shown in Fig. 7a ($\rho = 0.15$ mm, $d = 0.4$ mm and 0.8 mm) using the same resonance testing machine as described in the preceding section. Crack growth was monitored by means of the potential drop technique. The starter notch and a pair of shallow grooves on each side of the notch as shown in Fig. 9a were spark eroded into the specimen. The grooves were used to position the potential drop probes accurately. Five specimens were successfully tested at stress ratios $R = -1$, $R = 0$ and $R = 0.5$ as specified in Table 4. In order to avoid slack for $R < 0$, specimens with threaded heads were used; see Fig. 7a.

After initiating a fatigue crack at the notch root and propagating it to a depth of 0.2–0.3 mm, the notch was removed by machining away a layer of thickness d from the specimens as shown in Fig. 9b. Only specimen 3 was tested until failure without intermediate removal of the

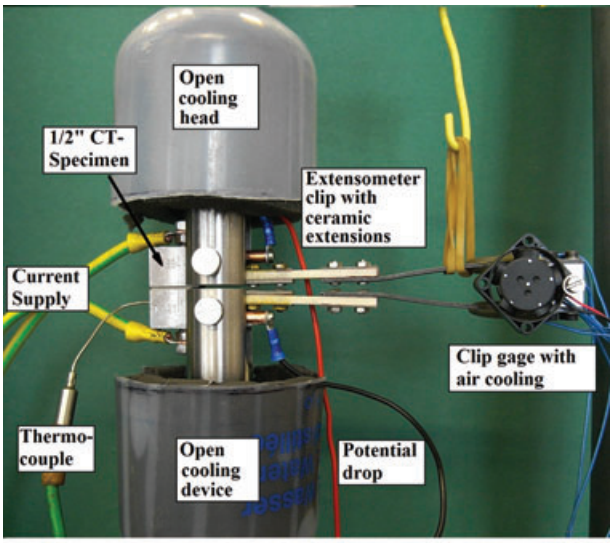

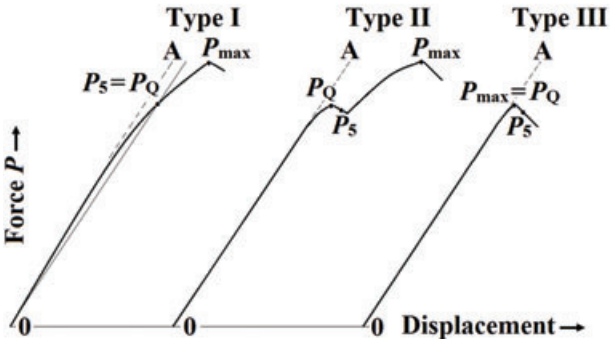

Fig. 5 (a) Setup for measurement of fracture toughness. (b) P_Q established from the force versus crack opening displacement diagram.[15]

Table 3 Fracture toughness data for ductile cast iron EN-GJS-400-18-LT

Specimen	T (°C)	$K_{J_{Ic}}$ (MPa$\sqrt{m}$)	$K_{P_{max}}$ (MPa$\sqrt{m}$)	K_Q(MPa$\sqrt{m}$)
SE(B)	22	81	33	23
SE(B)	22	72	30	24
C(T)	25	72	39	20
C(T)	2	68	39	22
C(T)	−19	69	46	30
C(T)	−38	79	47	26

notch. Table 4 summarizes the test conditions of the five different specimens, where 'i' signifies the crack initiation phase and 'p' the subsequent propagation phase.

Potential drop technique

The specimens were subjected to a direct current of 10 amperes, and the potential drop across the fatigue crack was measured with probes located at a distance $y = 2$ mm from the crack plane; see Figs 9 and 10. The specimen temperature was continuously monitored (using a thermocouple) to be able to compensate for its influence on the electrical resistance of the specimen. A computer program collected the elapsed number of cycles, the potential drop signal, the load amplitude and the temperature. As it was necessary to measure crack increments of the order of micrometres, a highly sensitive potential drop equipment was used. Potential drop was measured at the maximum load of the cycle, to make sure that the crack was fully open. A mean value was calculated every 660 cycles using a total of 200 subsequent potential drop measurements.

A relationship between the electrical potential drop and the crack depth may be obtained analytically, numerically or experimentally. Johnson[20] proposed a closed form analytical solution for the potential drop V across a single edge crack of depth a in a finite plate of width W normalized with respect to the potential drop V_0 across a single edge crack of depth a_0, namely

$$\frac{V}{V_0} = \frac{\cosh^{-1}\left\{\dfrac{\cosh\dfrac{\pi y}{2W}}{\cos\dfrac{\pi a}{2W}}\right\}}{\cosh^{-1}\left\{\dfrac{\cosh\dfrac{\pi y}{2W}}{\cos\dfrac{\pi a_0}{2W}}\right\}}. \tag{4}$$

Here y denotes the distance between the probes and the crack plane, cf. Fig. 10. Johnson's equation is also a good approximation of the potential drop across a sharp notch with a root crack as shown in Fig. 10, provided that a is replaced by $d + a$ and a_0 by d. Introducing the normalized potential drop *increase*,

$$u = \frac{V - V_0}{V_0}, \tag{5}$$

and solving (the modified) Eq. (4) for the crack depth, Mann et al.[21] obtained

$$a = \frac{2W}{\pi}\cos^{-1}\left\{\frac{\cosh\dfrac{\pi y}{2W}}{\cosh\left[(u+1)\cosh^{-1}\left(\dfrac{\cosh\dfrac{\pi y}{2W}}{\cos\dfrac{\pi d}{2W}}\right)\right]}\right\} - d. \tag{6}$$

This equation may be also used for the single edge crack in Fig. 10, where the notch has been removed, provided that d is replaced by the initial crack depth a_i, a by Δa and W by $W-d$. An application of Eq. (6) to specimen 6p is shown in Fig. 11, where u and a have been plotted against the number of load cycles.

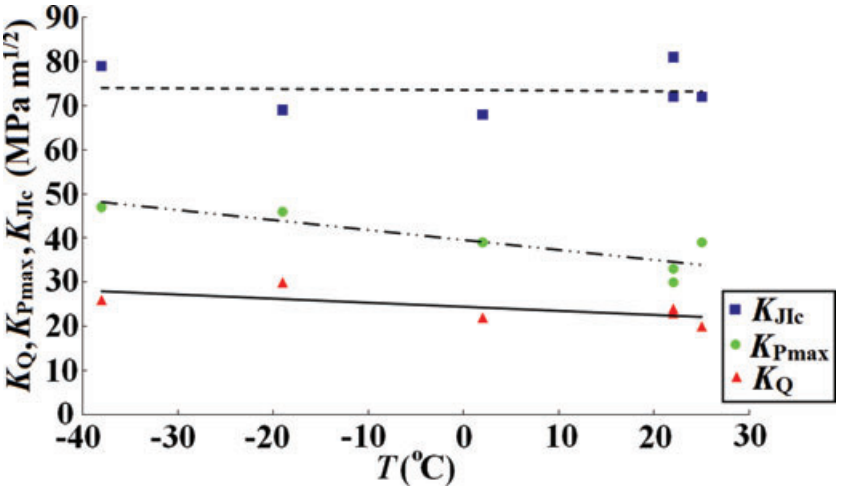

Fig. 6 Fracture toughness versus temperature for ductile cast iron EN-GJS-400-18-LT.

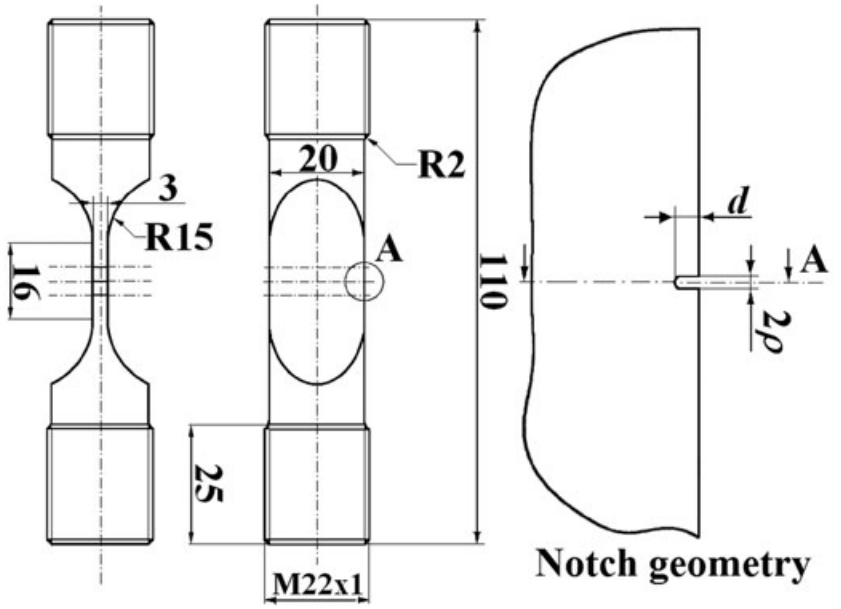

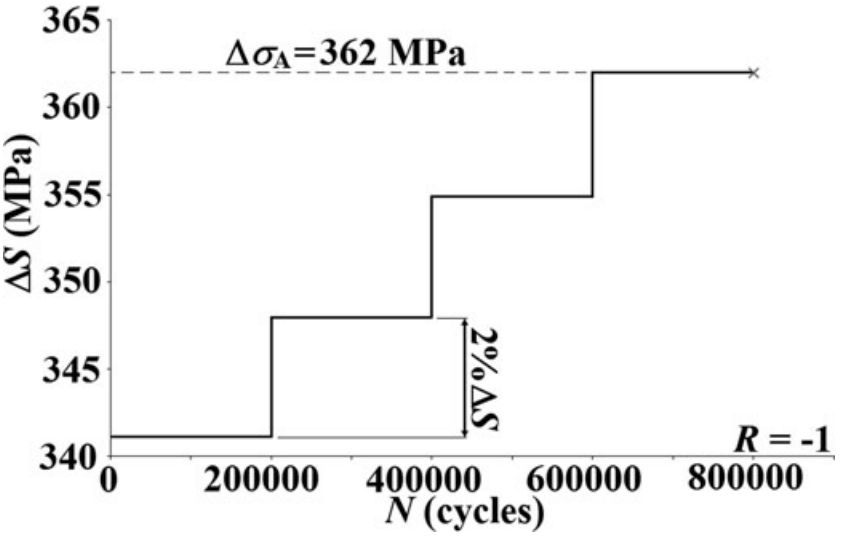

Fig. 7 (a) Plain ($d = 0$) or notched ($d > 0$) single-edge notch tensile specimen for fatigue testing and (b) load-increasing procedure for a plain specimen at $R = -1$.

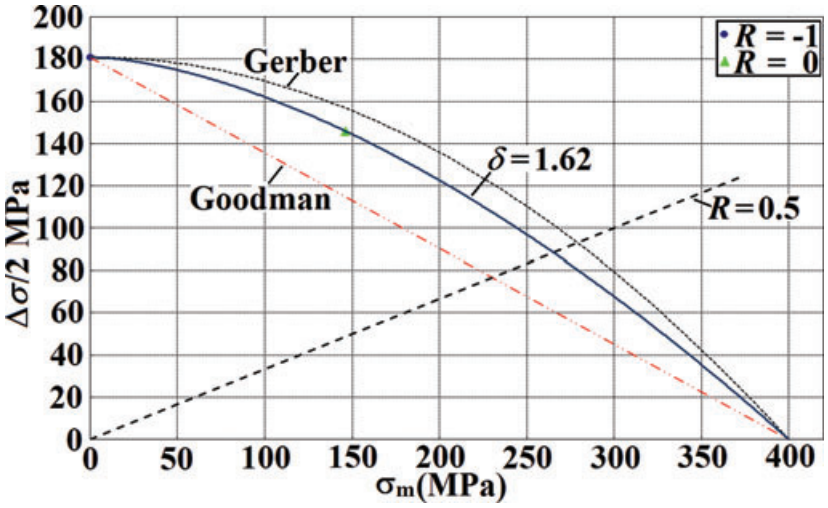

Fig. 8 Haigh diagram showing experimental data and (modified) Goodman and Gerber lines for ductile cast iron EN-GJS-400-18-LT.

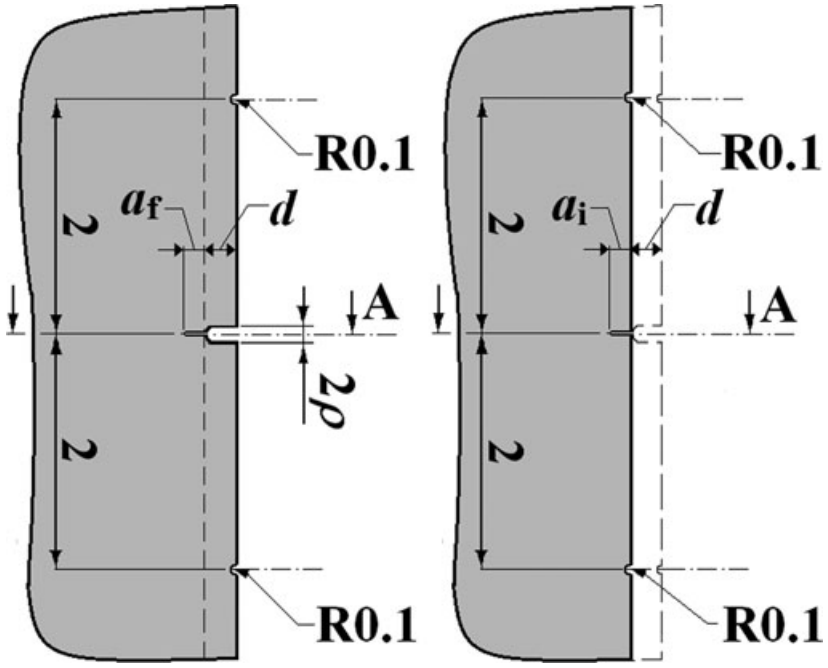

Fig. 9 (a) Crack initiated at root of starter notch; end of stage 'i'. (b) Cracked specimen after machining away the starter notch; beginning of stage 'p'.

Pre-cracking and FCG testing

In order to initiate and propagate a fatigue crack from the notch root at the least possible stress amplitude (= notched fatigue limit), a low amplitude was applied at the beginning of the test. The stress level was automatically increased by 2% every 100 000 cycles, as long as $u < 0.005$ within a block of load cycles; cf. Fig. 7b. After $u = 0.005$ had been reached, pre-cracking was controlled manually and stopped, when the crack at the notch root had become 0.2–0.3 mm deep; cf. Table 4. The notch was then removed as shown in Fig. 10.

The initiated cracks were marked by heat tinting at 250 °C for 4 h; see Fig. 12. After that, to determine again the minimum stress amplitude necessary to propagate the 0.2–0.3 mm deep initial crack, the same increasing–loading procedure as explained above was used for testing the plain cracked specimens. After the crack had become 0.5 mm deep, the stress amplitude was manually reduced until the crack stopped growing. Thereafter, the procedure was repeated to establish the threshold for crack growth, and finally constant amplitude loading was applied to propagate the crack, until this had grown to about half the width of the specimen.

The initial and final crack depths were measured under a microscope after breaking the specimen open, cf. Fig. 12. Intermediate crack depths, between test phases as specified in Table 4, have been measured on the lateral surface of the specimen by means of a travelling microscope.

Table 4 Stress ratio, notch depth and initial and final crack depths of subsequent crack initiation and propagation phases of the different specimens

Specimen	Reference	R	d (mm)	a_i (mm)	a_f (mm)
2i	D7894-9a	−1	0.4	0	0.31
2p	D7894-9b+c	0	0	0.31	7.98
3i	D7894-10a	−1	0.8	0	1.54
3p	D7894-10b	−1	0.8	1.54	1.64
3p	D7894-10c	−1	0.8	1.64	9.12
4i	D7894-11a	−1	0.8	0	0.26
4p	D7894-11b	0	0	0.26	1.78
4p	D7894-11c	0	0	1.78	8.65
6i	D7894-13a	0	0.8	0	0.19
6p	D7894-13b	0	0	0.19	1.94
6p	D7894-13c	0	0	1.94	10.25
8i	D7894-15a	−1	0.8	0	0.30
8p	D7894-15b	0.5	0	0.30	1.94
8p	D7894-15c	0.5	0	1.94	10.34

FCG OF SHORT AND LONG CRACKS

Crack depth analysis

The relative potential drop increase, u, was converted into crack depth, a, by means of Eq. (6). Figure 13 shows the crack depths, calculated from successive potential drop measurements, plotted against the number of cycles, N, for a short segment of the loading history of specimen 6p. As can be seen from the figure, the crack depth exhibits scatter, which is mainly due to (small) irregularities in the potential drop signal. This scatter can be much reduced by suitable averaging of crack depths. Thus, a straight line was fitted to twelve successive calculated crack depths, as presented in Fig. 13. The 'representative' (N_j, a_j) was taken at the middle of the line segment. This procedure was repeated by successively moving one data point ahead until all data had been covered. A line segment with a negative slope was neglected. Figure 13 shows three fitted line segments and three successive crack depths (a_j, a_{j+1}, a_{j+2}) computed in the middle of each line segment. After reducing the scatter, the resolution of the crack depth was better than 1 μm.

FCG rate against the stress intensity range

The crack growth rate was computed as $\mathrm{d}a/\mathrm{d}N = \Delta a/\Delta N$, where $\Delta N = N_{j+n} - N_j$ and $\Delta a = a_{j+n} - a_j$, respectively, as shown in Fig. 14. As the ASTM standard[22] recommends using Δa 10 times larger than the minimum resolution, n was chosen so that $\Delta a \geq 10$ μm. The representative crack depth was taken to be $a = (a_j + a_{j+n})/2$, and the associated stress intensity range was computed as

$$\Delta K = F \Delta S \sqrt{\pi a}, \tag{7}$$

where F is the crack geometry factor and ΔS the gross nominal stress range. For a single edge crack tension specimen, Tada et al.[23] proposed

$$F = \left(\frac{2W}{\pi a}\tan\frac{\pi a}{2W}\right)^{1/2} \times \left[\frac{0.752 + 2.02\left(\frac{a}{W}\right) + 0.37\left(1 - \sin\frac{\pi a}{2W}\right)^3}{\cos\frac{\pi a}{2W}}\right]. \tag{8}$$

This is also a good approximation of the geometry factor of a crack at the root of a notch as shown in Fig. 10, provided that a is replaced by $d + a$.

FCG rates as functions of the stress intensity range for load ratios $R = -1$, 0 and 0.5 are presented in Fig. 15a–c,

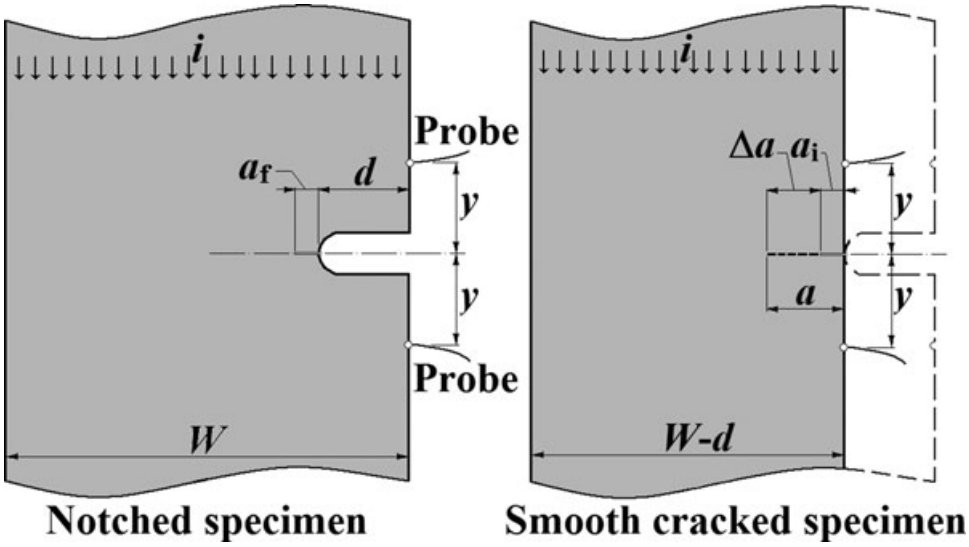

Fig. 10 Single-edge notch tension specimen instrumented for potential drop crack growth measurement.

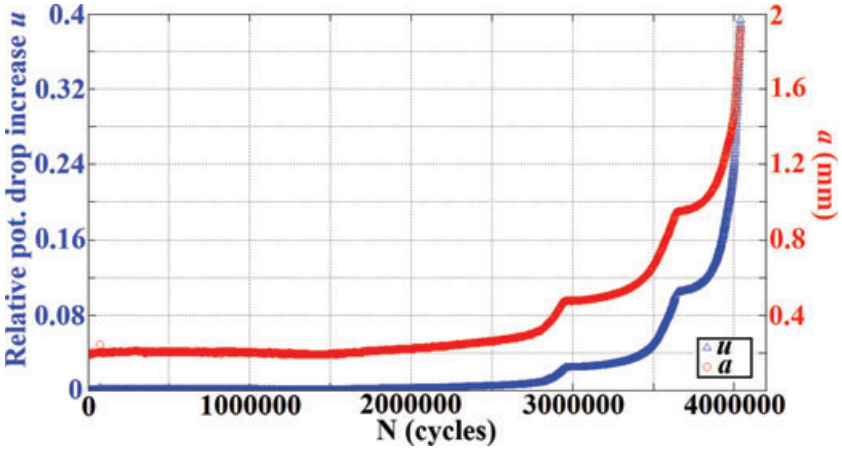

Fig. 11 Relative potential drop increase, u, and crack depth, a, for specimen 6p as functions of the number of load cycles.

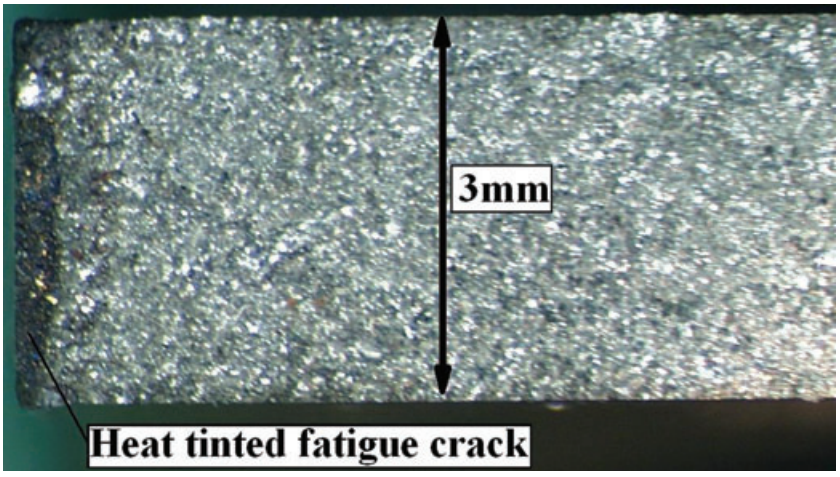

Fig. 12 Heat tinted initial fatigue crack after removal of the starter notch.

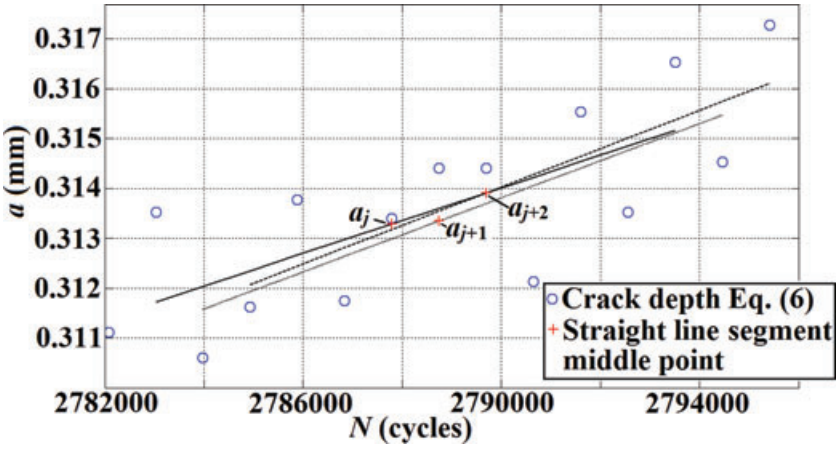

Fig. 13 Averaging of crack depths calculated from potential drop measurements.

where the crack depth range associated with a given set of test data has also been specified. Whereas long cracks have a well-defined threshold, this is not the case for short cracks. Indeed, two of the specimens, namely, 2p and 4p, exhibit 'fish-hook' behaviour, where the crack growth rate has a minimum below the long-crack threshold. Such anomalous behaviour of sub-millimetre cracks in cast iron EN-GJS-400-18-LT has not been reported before, although the FCG properties of this material have been investigated in several studies.[2,8,13] According to Dowling[18] and Suresh,[24] sub-threshold fatigue-crack growth, including 'fish-hook' behaviour, should be expected for cracks smaller than (a multiple of) the micro-structural length-scale for a variety of alloy systems with crack retardation as the crack front approaches and traverses a micro-structural barrier and subsequent acceleration. The

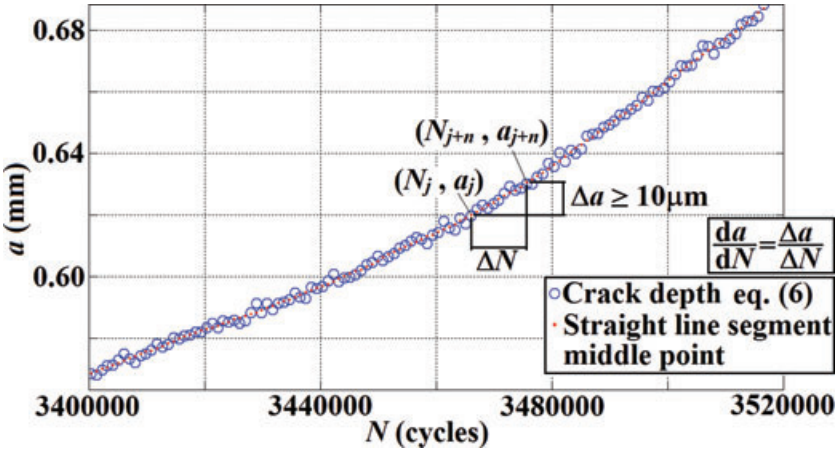

Fig. 14 Crack depths calculated from potential drop measurements (○) and averaged crack depths (+).

characteristic length scales of ductile cast iron, cf. Fig. 1, are given by the ferrite grain size and the graphite nodule spacing, both in the range 50–100 μm. Therefore, regular 'long-crack' growth should only be expected for cracks deeper than 0.5 mm, say.

In Fig. 15b and c have been included crack growth data from an investigation by Hübner et al.,[8] where a 10 mm × 20 mm × 100 mm three-point bend specimen with an edge crack deeper than 2 mm was used. At $R = 0.5$, there is good agreement with the present investigation except for $\Delta K > 10$ MPa$\sqrt{\text{m}}$, where WK2 (cf. Table 2) exhibits a marked increase in da/dN. At $R = 0.1$, WK2 has a slightly higher threshold value than specimens 2, 4 and 6 of the present investigation at $R = 0$. Moreover, WK2 has a marked increase in da/dN for $\Delta K >$ 15 MPa$\sqrt{\text{m}}$. The higher crack growth rates of WK2 for $K_{\max} >$ 15–20 MPa$\sqrt{\text{m}}$ have been attributed to incipient plastic failure of the net section of the three-point bend specimen.

An equivalent stress intensity range,

$$\Delta K_{\text{eq}} = F\Delta S\sqrt{\pi(a + a_0)}, \tag{9}$$

has been used in an attempt to unify the description of short and long FCG.[5,21,24,25,26] Applying this equation, with the 'intrinsic' crack depth

$$a_0 = \frac{1}{\pi}\left[\frac{\Delta K_{\text{th}}}{1.122\Delta\sigma_{\text{A}}}\right]^2, \tag{10}$$

to the present crack growth data yields the results shown in Fig. 16a–c, where da/dN has been plotted against ΔK_{eq}. Although short-crack data points are now slightly closer to long-crack data points, short cracks still exhibit anomalous behaviour with growth rates in the range of 0.01–1 nm/cycle down to $\Delta K_{\text{eq}} \approx 0.6\Delta K_{\text{th}}$. In particular, the 'fish-hook' remains. The 'intrinsic' crack model is an empirical attempt to take sub-threshold short-crack growth into account. However, its lack of microstructural data, as well as its simple mathematical structure, makes it unable to explain or predict the fish-hook effect.

Long-crack data were used to determine the parameters of the equation proposed by Klesnil and Lukáš[27],

$$\frac{\text{d}a}{\text{d}N} = C\left(\Delta K_{\text{eq}}^m - \Delta K_{\text{th}}^m\right), \tag{11}$$

by means of a least-squares fit. The material parameters C, m and ΔK_{th} are given in Table 5 for the different stress ratios used in the tests. At $R = 0$, C and m have been determined for specimen 4p, which exhibits the highest and thus most conservative growth rate data of the three specimens investigated at this load ratio.

The threshold stress intensity range and its load ratio dependence

A simple crack-closure model, used by Mann[28] for modelling FCG in aluminium alloys, assumes the stress intensity range of the fully open crack, i.e. $\Delta K_{\text{eff}} = K_{\max}$-$K_{\text{op}}$ for $R \le R_{\text{op}}$ and $\Delta K_{\text{eff}} = K_{\max}$-$K_{\min}$ for $R \ge R_{\text{op}}$, to have a constant threshold, $\Delta K_{\text{eff,th}}$. Eliminating K_{op}, the stress intensity factor above which the crack remains open, yields

$$\Delta K_{\text{th}} = \Delta K_{\text{eff,th}}(1 - R)/(1 - R_{\text{op}}) \text{ for } R \le R_{\text{op}}, \tag{12a}$$

$$\Delta K_{\text{th}} = \Delta K_{\text{eff,th}} \text{ for } R \le R_{\text{op}}. \tag{12b}$$

In this study, $\Delta K_{\text{eff,th}}$ has been assumed to be equal to the threshold stress intensity range, ΔK_{th}, at the highest applied load ratio, $R = 0.5$. $R_{\text{op}} = 0.15$ is then obtained by least-squares fitting of Eq. (12a) to the experimentally determined ΔK_{th} at $R = -1$ and $R = 0$ as given by Table 5. More fatigue experiments are recommended

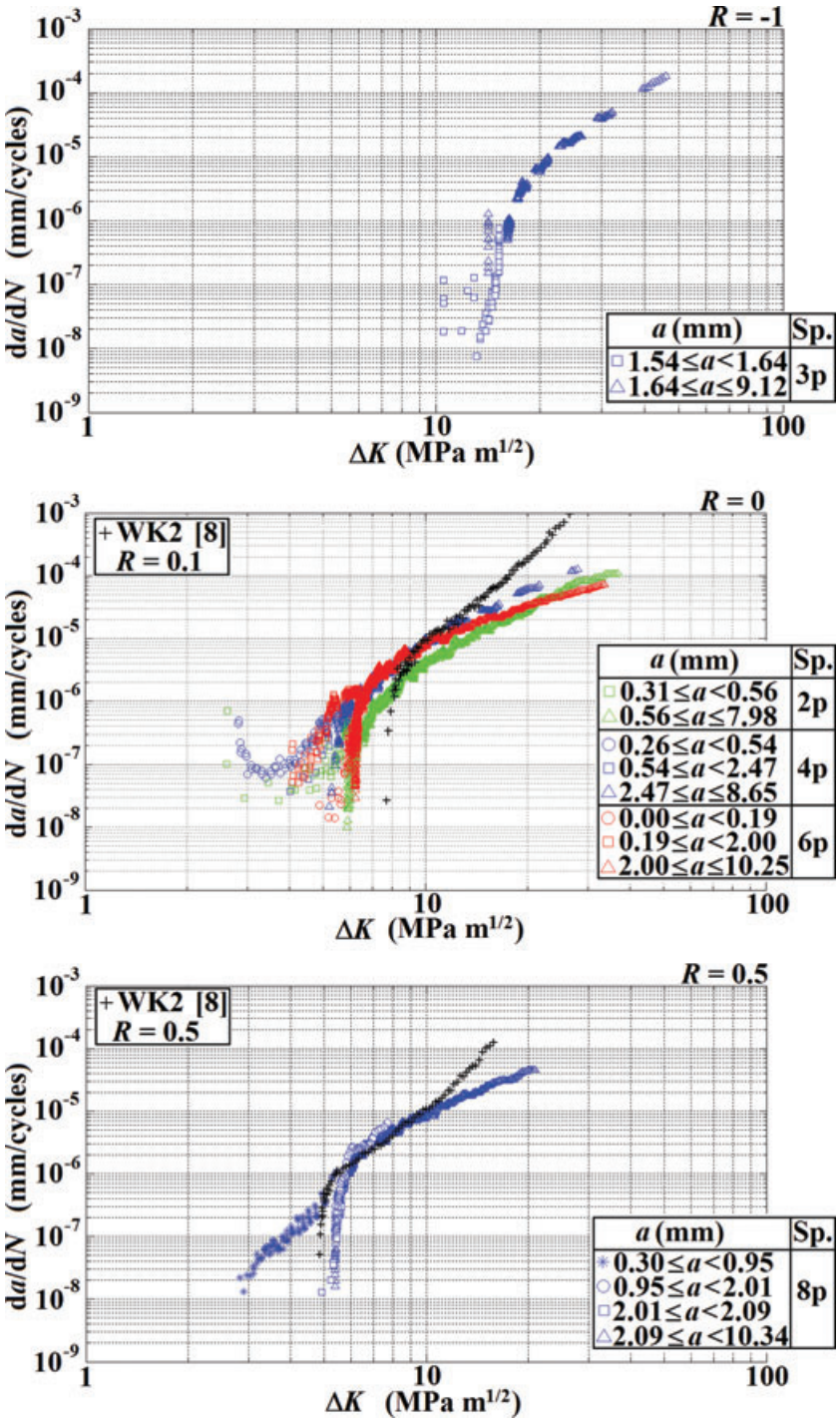

Fig. 15 Fatigue crack growth rate for ductile cast iron EN-GJS-400-18-LT as a function of the stress intensity range at (a) $R = -1$, (b) $R = 0$, and (c) $R = 0.5$.

to establish whether ΔK_{th} remains constant for $R > R_{op}$. Hübner et al.[8] reported $\Delta K_{th} = 7.8$, 6.5 and 4.9 MPa$\sqrt{m}$ for WK2 at $R = 0.1$, 0.3 and 0.5, respectively. Fitting Eq. (12a) to these data at $R = 0.1$ and $R = 0.3$ and (again) assuming $\Delta K_{eff,th} = \Delta K_{th}(R = 0.5)$ yields $R_{op} = 0.45$. ΔK_{th} versus R for the two investigations is shown in Fig. 17. Although there is some disagreement between data in the range $R = 0$–0.5, the (bi-linear) fits show reasonable overall agreement in the range $R = -1$–0.5. It should be kept in mind that Hübner et al. used three-point bend specimens, whereas edge-cracked tension specimens were tested in this study. Continued testing is needed to ensure a more complete and robust database for FCG in ductile cast iron EN-GJS-400-18-LT.

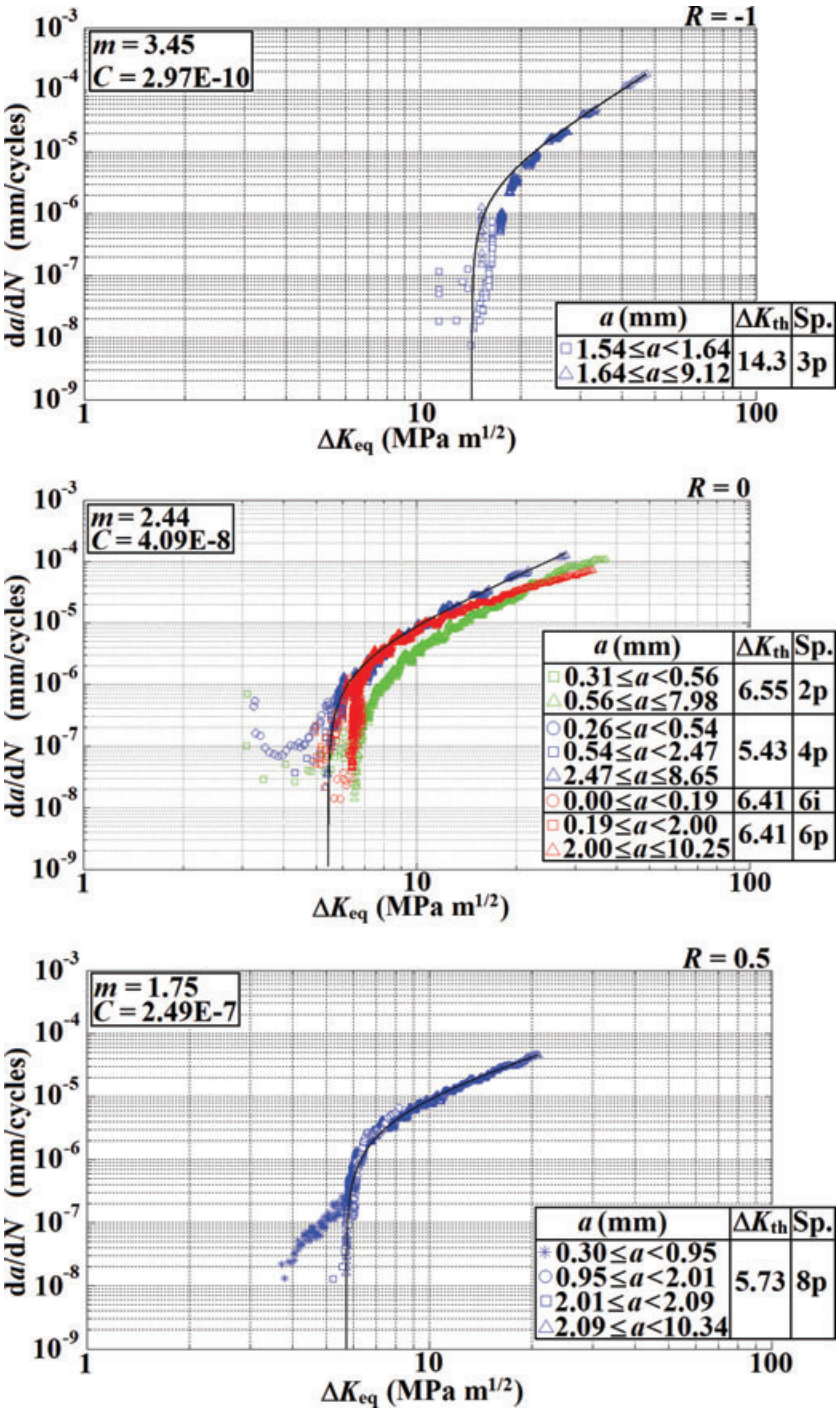

Fig. 16 Fatigue crack growth rate for ductile cast iron EN-GJS-400-18-LT as a function of the equivalent stress intensity range at (a) $R = -1$, (b) $R = 0$, and (c) $R = 0.5$.

CONCLUSIONS

Tensile, fracture toughness and FCG data from comprehensive tests on ductile cast iron EN-GJS-400-18-LT have been presented and critically assessed.

The tensile properties of the investigated casting fulfil the requirements of the European Standard EN 1563.[1] A comparison with tensile data for other GJS-400-type castings showed that tensile and yield strengths are nearly independent of mean graphite nodule diameters in the range 15–60 μm.

The fracture toughness of the investigated material was virtually constant from room temperature down to −40 °C.

As should be expected, the plain push–pull fatigue limit was found to be slightly below the plain fatigue limit under

Table 5 Fatigue properties of ductile cast iron EN-GJS-400-18-LT

Specimen	R	$\Delta\sigma_A^a$ (MPa)	ΔK_{th} (MPa$\sqrt{m}$)	a_0 (mm)	C^b	m	max ΔK^c (MPa$\sqrt{m}$)
3p	−1	362	14.3	0.396	2.97×10^{-10}	3.45	50
2p	0	292	6.55	0.127	–	–	–
4p	0	292	5.43	0.087	4.09×10^{-8}	2.44	30
6p	0	292	6.41	0.122	–	–	–
8p	0.5	177	5.73	0.266	2.49×10^{-7}	1.75	20

[a]Due to Fig. 8.
[b]Units in Eq. (11) are mm/cycle and MPa$\sqrt{m}$.
[c]Upper limit for C and m to be valid.

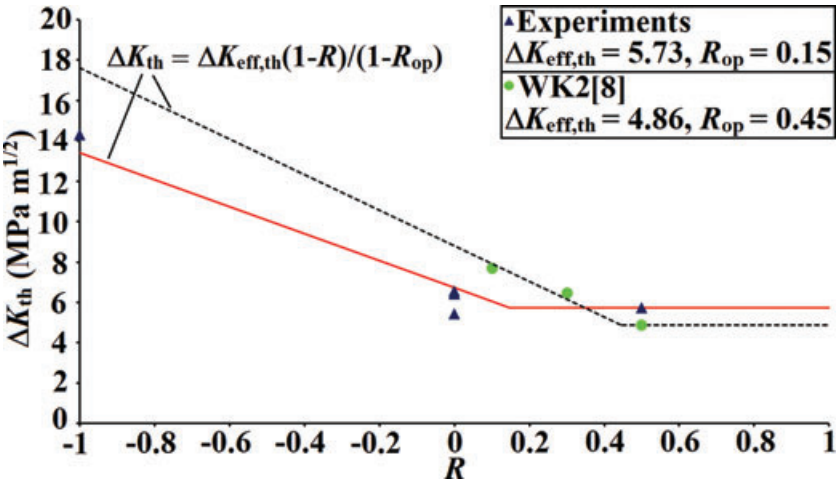

Fig. 17. R-ratio effect on ΔK_{th} for ductile cast iron EN-GJS-400-18-LT.

rotating bending stated in EN 1563. The weak mean-stress sensitivity of the fatigue limit was in agreement with that found by Kaufmann and Wolters[19] for ductile cast iron free from 'irregular' defects. A modified Gerber equation was used to model the mean-stress dependence of the fatigue limit.

FCG has been studied at $R = -1$, 0 and 0.5. To the knowledge of the authors, this is the first investigation of EN-GJS-400-18-LT at $R = -1$. Crack growth rates at $R = 0.5$ are in fair agreement with data from a previous study by Hübner et al.[8] for $\Delta K < 10$ MPa$\sqrt{m}$, whereas considerable deviation is observed at $R \approx 0$.

The threshold stress intensity range of long cracks (>1 mm) was determined for $R = -1$, 0 and 0.5 and fitted to a simple crack closure model. The load ratio dependence in the interval $R = 0$–0.5 of the present investigation is found to be weaker than that of Hübner et al.[8]

Short, sub-millimetre cracks were observed to grow at stress intensity ranges well below the long-crack threshold. An attempt to correct for short-crack behaviour by means of the intrinsic crack depth, a_0, slightly improved the agreement between da/dN versus ΔK for short and long cracks, but did not eliminate the short-crack anomalies.

In view of the importance of ductile cast iron EN-GJS-400-18-LT in wind turbine design, it is recommended that experimental investigations of its FCG characteristics be continued, in particular for $R > 0.5$ and $R < 0$. Such experiments should be suitably instrumented for the determination of crack closure.

Acknowledgements

The authors would like to acknowledge financial support by MATSINT, a research program under the auspices of the Research Council of Norway. Thanks are also due to Alstom Wind for financing the experimental activities, to Vestas Wind Systems for providing the cast material, and to Dr. Hübner for providing fatigue crack growth and fracture toughness data from previous work at TU Bergakademie Freiberg.

REFERENCES

1 European Standard EN 1563:1997. (1997) Founding–Spheroidal graphite cast iron, CEN.
2 Verdu, C., Adrien, J. and Buffière, J. Y. (2007) Three-dimensional shape of the early stages of fatigue cracks nucleated in nodular cast iron. *Mater. Sci. Eng. A* **483–484,** 402–405.

3 Murakami, Y. (2002) *Metal Fatigue: Effect of Small Defects and Non Metallic Inclusions*. Elsevier, Amsterdam, [ISBN: 0-08-044064-9].

4 Nadot, Y., Mendez, J. and Ranganathan, N. (2003) Influence of casting defects on the fatigue limit of nodular cast iron. *Int. J. Fatigue* **26,** 311–319.

5 Fjeldstad, A., Wormsen, A. and Härkegård, G. (2007) Simulation of fatigue crack in components with random defects. *Engng. Fract. Mech.* **75,** 1184–1203.

6 Beretta, S., Blarasin, A., Endo, M., Giunti, T. and Murakami, Y. (1997) Defect tolerance design for automotive components. *Int. J. Fatigue* **19**(4):319–333.

7 Skallerud, B., Iveland, T. and Härkegård, G. (1993) Fatigue life assessment of aluminium alloys with casting defects. *Engng. Fract. Mech.* **44,** 857–874.

8 Hübner, P., Schlosser, H., Pusch, G. and Biermann, H. (2007) Load history effects in ductile cast iron for wind turbine components. *Int. J. Fatigue* **29,** 1788–1796.

9 Tokaji, K., Ogawa, T. and Shamoto, K. (1994) Fatigue crack propagation in spherical graphite cast iron with different microstructures. *Int. J. Fatigue* **16,** 344–350.

10 Cavallini, M., Bartolomeo Di O. and Iacoviello, F. (2007) Fatigue crack propagation damaging micromechanisms in ductile cast irons. *Engng. Fract. Mech.* **75,** 694–704.

11 Shirani, M. and Härkegård, G. (2009) Fatigue crack growth simulation in components with random defects. *J. ASTM Int.* **6**, doi: 10.1520/JAI102542.

12 Berdin, C., Dong, M. J. and Prioul, C. (2001) Local approach of damage and fracture toughness for nodular cast iron. *Engng. Fract. Mech.* **68,** 1107–1117.

13 Clement, P., Angeli, J. P. and Pineau, A. (1984) Short crack behaviour in nodular cast iron. *Fatigue Engng. Mater. Struct.* **7,** 251–265.

14 Yasufumi, I. and Tomokazu, M. (1982) Effect of side grooves on the elastic-plastic stress state of fracture toughness specimens– three-dimensional finite element analysis. *Engng. Fract. Mech.* **16,** 659–668.

15 ASTM E1820-09. (2010) Standard test method for measurement of fracture toughness. In: *Annual book of ASTM Standards*. ASTM E1820-09, West Conshohocken.

16 Denk, J. and Amhof, S. (1996) Determination of the high cycle fatigue strength with a load-increasing single-specimen technique. In: *Fatigue 96: Proceedings of the Sixth International Fatigue Congress held in Berlin, Germany, 6–10 May 1996*. (Edited by G. Lütjering, & H.Nowack) EMAS Publishing, Sheffield, (ISBN 0 08 0422683).

17 Hassan, T. and Liu, Z. (2001) On the difference of fatigue strengths from rotating bending, four-point bending, and cantilever bending tests. *Int. J. Press. Vessels Pip* **78,** 19–30.

18 Dowling, N. E. (2007) *Mechanical Behaviour of Materials: Engineering Methods for Deformation, Fracture and Fatigue*. 3rd edn. Prentice Hall, NJ.

19 Kaufmann, H. and Wolters, D. (2002) Zyklische Beanspruchbarkeit dickwandiger Bauteile aus ferritischem Gusseisen mit Kugelgraphit. *Konstruieren+Giessen* **27,** 4–27.

20 Johnson, H. H. (1965) Calibrating the electric potential method for studying slow crack growth. *Mater. Res. Stand.* **5,** 442–445.

21 Mann, T., Härkegård, G. and Stärk, K. (2007) Short fatigue crack growth in aluminium alloy 6082-T6. *Int. J. Fatigue* **29,** 1820–1826.

22 ASTM E647-08. (2008) Standard test method for measurement of fatigue crack growth. In: *Annual book of ASTM standards* ASTM, West Conshohocken.

23 Tada, H., Paris, P. C. and Irwin, G. R. (2000) *The Stress Analysis of Cracks Handbook*. 3rd edn. Professional Engineering Publishing Limited, Bury St. Edmunds and London.

24 Suresh, S. (1998) Small fatigue cracks.*Fatigue of Materials*. 2nd edn. Cambridge University Press, Cambridge, Ch. 15.

25 El Haddad, M. H., Topper, T. H. and Smith, K. N. (1979) Prediction of non-propagating cracks. *Engng. Fract. Mech.* **11**, 573–584.

26 Härkegård, G. (1981) An effective stress intensity factor and the determination of the notched fatigue limit. In: *Fatigue Thresholds*, Vol. II, (Edited by J. Bäcklund *et al*. EMAS, Warley, UK, pp. 867–879.

27 Klesnil, M. and Lukáš, P. (1972) Influence of strength and stress history on growth and stabilisation of fatigue cracks. *Engng. Fract. Mech.* 4, 77–92.

28 Mann, T. The influence of mean stress on fatigue crack propagation in aluminium alloys. *Int. J. Fatigue* 29, 1393–1401.